

High-Performance Training by Exploiting Hot-Embeddings in Recommendation Systems

Muhammad Adnan[†]Yassaman Ebrahimzadeh Maboud[†]University of British Columbia[†]Divya Mahajan^{*}Microsoft Inc.^{*}Prashant J. Nair[†]

Abstract—Recommendation models are commonly used learning models that suggest relevant items to a user for e-commerce and online advertisement-based applications. Current recommendation models include deep-learning based (DLRM) and time-based sequence (TBSM) models. These models use massive embedding tables to store numerical representation of item’s and user’s categorical variables (memory bound) while also using neural networks to generate outputs (compute bound). Due to these conflicting compute and memory requirements, the training process for recommendation models is divided across CPU and GPU for embedding and neural network executions, respectively. Such a training process naively assigns same level of importance to each embedding entry. This paper observes that some training inputs and their accesses into the embedding tables are heavily skewed with certain entries being accessed up to $10000 \times$ more.

This paper tries to leverage skewed embedded table accesses to efficiently use the GPU resources during training. To this end, this paper proposes a *Frequently Accessed Embeddings* (FAE) framework that provides three key features. First, it exposes a dynamic knob to the software based on the GPU memory capacity and the input popularity index, to efficiently estimate and vary the size of the *hot* portions of the embedding tables. These hot embedding tables can then be stored locally on each GPU. FAE uses statistical techniques to determine the knob, which is a threshold on embedding accesses, without profiling the entire input dataset. Second, FAE pre-processes the inputs to segregate hot inputs (which only access hot embedding entries) and cold inputs into a collection of hot and cold mini-batches. This ensures that a training mini-batch is either entirely hot or cold to obtain most of benefits. Third, at runtime FAE generates a dynamic schedule for the hot and cold training mini-batches that minimizes data transfer latency between CPU and GPU executions while maintaining the model accuracy. The framework execution then uses the GPU(s) for hot input mini-batches and a baseline CPU-GPU mode for cold input mini-batches. Overall, our framework speeds-up the training of the recommendation models on Kaggle, Terabyte, and Alibaba datasets by $2.34 \times$ as compared to a baseline that uses Intel-Xeon CPUs and Nvidia Tesla-V100 GPUs, while maintaining accuracy.

I. INTRODUCTION

Training large-scale machine-learning models has garnered widespread interest due to their compute and memory requirements [4–8]. Recommender models form an important class of machine learning algorithms. Well-trained recommender models are vital for industry players like Netflix [9], Facebook [10], and Amazon [11] to offer a targeted user experience. Unfortunately, training production-scale recommendation models require memory resources [1, 3] and massive computation [12–14]. This is because recommender models contain a combination of large Embedding Tables and Neural Networks as shown in Figure 1. While the neural network components in these models can efficiently use GPU compute, the large embedding tables (10s of GBs in size) often cannot fit within GPU memories [15, 16]. Thus, these models typically use a combination of CPUs and GPUs during the training pro-

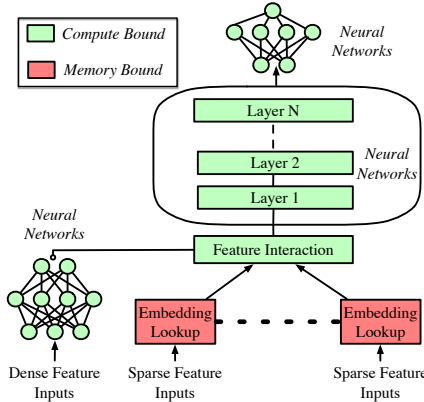


Fig. 1: Typical recommender model [1–3]. These models comprise of an interconnection of compute-bound Neural Networks like DNNs and MLPs in tandem with the memory-bound (size and bandwidth) Embedding Tables.

cess [17–19], with the CPUs providing the memory capacity for Embedding Tables. Thus, one cannot fully utilize the GPUs to accelerate the embedding portion of these models. This paper aims to mitigate this concern and improve performance.

Proposals such as reduced-precision [20, 21], sparse [22], and compressed [16, 23–25] data techniques are often used to reduce memory footprint and bandwidth requirements. Ideally, efficiently utilizing memory without changing the precision or sparsity of data and in turn not incurring any compression/decompression overheads is preferable. This paper focuses one such technique of *data placement and management* that exploits *access-patterns of embedding tables* for real-world datasets to efficiently train large recommender models.

Figure 2 shows the size of the embedding tables for *three real-world datasets* [26–28] across two open-source recommender models, “Deep Learning Recommendation Model for Personalization and Recommendation Systems” (DLRM) [1] and “Time-based Sequence Model for Personalization and Recommendation Systems” (TBSM) [3]. Figure 2 also lists the memory capacities of modern GPU devices. We observe that, even on a high-end server class GPU device such as Nvidia Tesla-V100, recommendation models may not be able to fit the embedding tables (for some datasets) entirely within the GPU device memory. As model size of machine learning algorithms evolves, the size of these embedding tables is only expected to increase [16, 29]. This is because large embedding tables can track a greater degree of user preferences [15].

Therefore, currently the state of the art is to train recommendation-system models with CPUs handling the embedding tables and GPUs performing data parallel training for

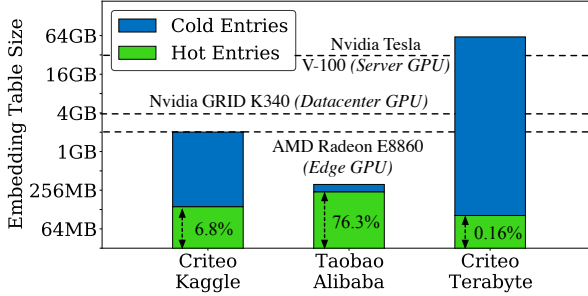


Fig. 2: Embedding table sizes for Criteo Kaggle [26], Taobao Alibaba [27], and Criteo Terabyte [28] Datasets. The graph also shows the proportion of frequently accessed (hot) portions of the embedding table, essentially entries that have accesses greater than 10^{-5} , 10^{-6} , 10^{-5} of the total accesses, respectively. We observe that, while embedding tables can be *10s of GBs* in size, hot portions are often *under 256MB* in size.

the neural network portions of the models. Alternatively, we can train using Model Parallelism by using only GPUs. Model parallelism is usually deployed for very large models that cannot fit on a single device and needs to be split across devices. Each split often exhibits a high computational intensity and utilizes resources effectively. Therefore, using multiple GPUs simply for memory capacity is not optimal, as the number of GPU devices per computer node are usually fixed and scarce. Additionally, GPU-GPU communication costs for some of these models is 60% on average [30–32]. Thus, in practice, it is common to see CPUs providing its high-capacity memory system for executing the embedding layers, while the GPUs executes the massively parallel neural network layers [17].

Figure 1 shows the commonly used training model for recommender system. These systems have two types of inputs, namely dense and sparse. Dense inputs are continuous inputs (such as time of day, location of users, etc.) that feed directly into the neural network layers. Sparse inputs are specific to each user and they typically denote specific preferences of the user (like the movie genre, choice of music, etc.). Several prior work has shown that certain sparse inputs are significantly more popular (or hot) than others and such inputs skew the embedding table accesses [33, 34]. Figure 2 highlights the size of the hot portion of the embedding table access by hot sparse inputs. To establish: an embedding entry is hot if it captures at least the specified percentage of the total accesses and a hot input is one that only accesses these hot entries. Even for a large dataset like Criteo Terabyte, the size of *hot* portions of embedding tables is only ~ 78 MB (compared to 61GB of the entire embedding table size) and easily fit within the memory of even a low-end GPUs. These hot indices account for 75% to 92% of the total accesses. Using this insight, we propose to store and execute the hot embedding entries locally on every GPU device. This would allow us to train the inputs that access only hot embedding entries in a “data parallel” fashion across GPUs. This would also enable us to mitigate the communication overheads in a distributed training setting. Any synchronization after the data-parallel mini-batch can now be performed in tandem with the neural network that was already

executing on all the GPUs (like the baseline).

Moving the hot embeddings into every GPU poses *four key challenges*. First, learning large models through distributed training uses a mini-batch of inputs at a time. Thus, if any input within the mini-batch accesses cold embeddings, there will be back and forth communication between the CPU and GPU for the mini-batch. Second, training *only* on hot or cold inputs can have an impact on accuracy. This is because, each of these inputs would only update the hot or cold portions of the embedding parameters. Third, as hot embeddings are scattered, all the GPUs and CPU would need to be synchronized after each data parallel execution. Fourth, the hotness of an embedding entry depends on the dataset and recommender model. Therefore, hotness needs to be re-calibrated for every model, dataset, and system configuration tuple.

To this end, this paper proposes the *Frequently Accessed Embeddings* (FAE) framework, a comprehensive framework to accelerate training of large recommender models whilst ensuring accuracy. This work makes the following contributions:

- 1) We intelligently allocate the hot embedding entries on every GPU device involved in the data-parallel distributed training task. This reduces the communication overhead for hot embedding entries (which account for most of the accesses) and also accelerate the embedding compute. The technique does not change the model or its training and exploits a runtime feature for higher performance.
- 2) We devise FAE, a comprehensive framework that has both static and runtime components to leverage the above insight and to provide high performance benefits. Statically, the FAE samples input dataset to determine the access patterns to embedding tables. Based on hot embedding access pattern information, the FAE pre-processes the input data and categorizes them into hot and cold categories. It ensures that an entire mini-batch for training exclusively accesses only hot or only cold portions of the embedding table to avoid back and forth communication.
- 3) The FAE framework employs statistical techniques to avoid traversing through both the input dataset and the embedding tables. This helps determine the hot embedding access threshold and the size of the hot embedding table while incurring extremely low overhead.
- 4) At runtime, the FAE framework intertwines executions of hot and cold input mini-batches across CPUs and GPUs to ensure the baseline training accuracy.

We evaluate our framework for a wide variety of deep learning based recommender models and real-world datasets. We compare the FAE optimized training with baseline where the embedding phase of the training executes on the CPU and the neural network on GPU. Results show that FAE achieve a performance improvement of $2.34\times$ (on average) over baseline for a 4 GPU training execution. Additionally, due to the reduced data transfer between CPU and GPU, FAE training consumes on average 6.7% less power per GPU. Thus, the FAE helps exploit popular inputs and hot embedding entries to efficiently utilize GPUs for recommender system training.

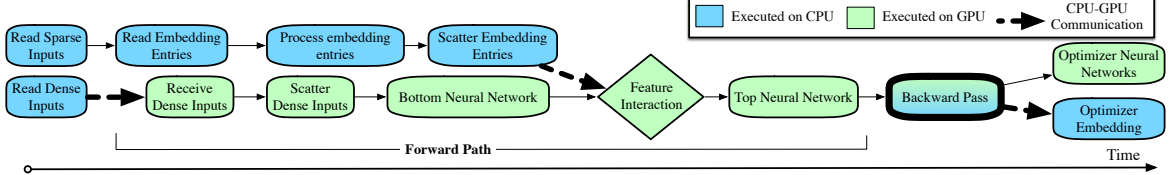


Fig. 3: Execution graph for deep learning based recommender model. In this graph we show the forward graph in detail, the backward pass is a mirror of forward and executes on CPU and GPU according to its forward counterpart. The current mode of training requires embedding storage, reading, and processing, on CPU, thus increasing the data transfer and also requiring the optimizer and weight update (which is otherwise well suited for GPU execution) to execute in CPU.

II. OVERVIEW AND CHALLENGES

Machine learning commonly employs data-parallel training with large mini-batch sizes to reduce the overall training time [35]. This mode often requires model replication across all the GPU devices, where each device executes different inputs within a mini-batch, and a post-execution synchronization to update the weights/parameters by the aggregated gradient values. However for recommendation models, training in a data-parallel fashion is unappealing as they use large embedding tables (in the embedding layer) in tandem with deep neural networks. Even beyond recommendation models, large embeddings are now being used to represent categorical features [29, 36]. The embedding layer component in a recommender model is highly memory and bandwidth intensive as these tables are of the order of 10's of GBs. Conversely, the Deep Neural Network and Multi-Layer Perceptron (MLP) components in the recommender model work on continuous features and therefore are more compute intensive. Below we discuss some background on training of these models.

A. State of the Art Recommender Model Training

Recommendation models can employ datasets that use large embedding tables that are capacity limited. To overcome this issue, as shown in Figure 3, past work executes the memory intensive embedding layer on the CPU and compute intensive top and bottom DNN layers on the GPUs. Figure 3 illustrates the flow of such a setup. Such a setup incurs data transfer overheads of intermediate results and gradients between the GPU and CPU devices after each type of execution, shown by the bold dotted lines in the graph. As the embedding layer is stored on the CPU, after the backward pass, the training optimizer (e.g. Stochastic Gradient Descent), which is a massively parallel operation, is also performed on the CPU. This approach naively assumes that all embedding entries have similar number of accesses and thus stores the entire embedding layer on the CPU. We observe that the accesses into the embedding tables are heavily skewed in *real world applications*. This is because some inputs are highly popular. For instance, for the Criteo Kaggle dataset [26] on DLRM, the top 6.8% of the embedding table entries get at least 76% of the total accesses. This paper leverages this insight to replicate the hot embedding entries on every GPU. This allows us to execute the entire training graph, shown in Figure 3, on the GPU for inputs which only access the hot embeddings. This optimization overcomes the limitations of the CPU embedding

setting for part of the inputs (hot inputs) by - (1) *accelerating embedding compute including the optimizer* through GPUs whilst being *within the memory capacity* of the device and (2) *eliminating the communication overheads* (gradients and activations) between CPU and GPU devices.

B. Challenges and Insights

To perform successful end-to-end training run without loosing accuracy, we require a comprehensive framework that has both static and runtime components. Before delving into the design details we analyze the properties and challenges of such a training execution. Below we discuss the insights that guide the design of our framework.

(1) Does moving the hot regions to the GPU suffice? As mentioned before, we store the hot regions of the embedding table in every GPU. However, as we know that machine learning training uses a mini-batch of inputs distributed across machines in a data parallel fashion. As shown in Figure 4, even if 99% of the inputs access hot embedding tables, as we increase the size of mini-batch the probability that the entire mini-batch accesses *only* the hot embedding tables decreases drastically. This is because some inputs in a large mini-batch may access cold embedding entries.

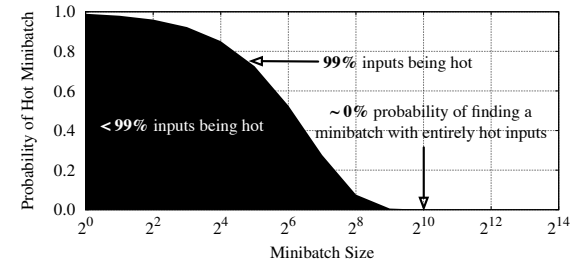


Fig. 4: Probability of creating a mini-batch with all hot inputs when the number of hot-inputs are 99% or lower. This reduces drastically as the mini-batch size increases as it is likely that at least one input in a large mini-batch is not hot and therefore classifies the entire mini-batch as not-hot.

Ideally, we require the entire mini-batch to access hot embedding entries. This is because, even a single input accessing cold embedding entries would end up in the critical path and stall execution as it tries to obtain its embedding entries from the CPU memory. To overcome this challenge, our framework comprises of a static component that performs input-dataset preprocessing and organizes mini-batches such

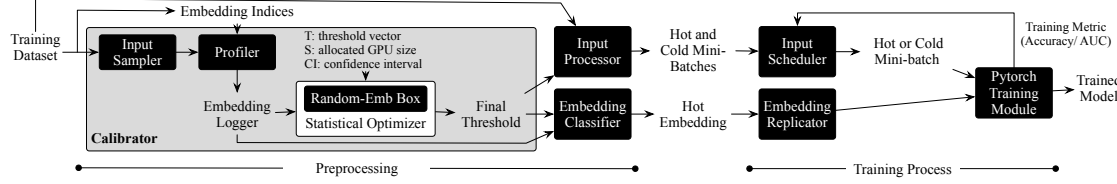


Fig. 5: The FAE framework. The Calibrator block forms the main pre-processing component which calculates the threshold for classifying hot embedding entries. This block uses random-sampling of input datasets and embedding tables to determine the best threshold for hot embedding entries. Threshold is used to classify inputs into hot and not-hot mini-batches. At runtime, the entire execution for hot input mini-batch happens in a data-parallel model which only utilizes all the model on the GPU to reduce training time and not-hot inputs executed as baseline. The Shuffle Scheduler uses feedback from the pytorch modules to determine how often hot and not-hot inputs need to be scheduled for training.

that they completely contain only hot or cold inputs. This preprocessing needs to be performed *only* once for every dataset and is stored in the preprocessed format for subsequent executions. For hot mini-batches, the framework performs the GPU-only pure data-parallel execution and for cold mini-batches the framework falls back onto the baseline mode.

(2) What constitutes a hot embedding entry? We have extensively discussed that certain regions of the embedding table are hot, however, the classification of an embedding entry as hot or cold is based on an access threshold. We expose this threshold as a knob to FAE to adjust how large the hot embedding tables can be based on both model and system specifications. We devise statistical techniques to determine the access threshold without scanning the entire dataset. Subsequently, we analyze only a sample of the accesses to estimate the size of hot embedding table. Using this information we can efficiently use a vector of thresholds and select the one that fits the embedding table into the allocated memory.

(3) How to maintain consistency between embedding tables scattered across devices? In our approach, copies of the hot embedding tables are replicated across all the GPU devices. The CPU also has hot embedding entries for baseline execution of cold inputs (cold inputs might access some hot embedding entries). To reduce the overhead of this synchronization, we perform all-reduce on all the gradients including both embedding and neural network layers over the fast NVLink interconnect. While this increases the size of the synchronized gradient, it is called *only* once and therefore incurs low communication costs. When moving execution from hot to cold mini-batches, or vice-versa, the hot embedding entries are updated on the CPU and GPU. To reduce the update overheads, our FAE has to be aware of this at runtime to minimize the transitions between hot and cold mini-batches.

(4) How to schedule hot and cold mini-batches? After data preprocessing, we have mini-batches that are either entirely hot or cold. Scheduling the entire hot mini-batches followed by cold mini-batches incurs the least embedding update overhead, however such a scheme can have an impact on the accuracy. This is because the hot mini-batches only update the hot embedding entries whereas the cold mini-batches sparsely cover more of the embedding table entries (both hot and cold). To tackle this issue, our framework, offers a runtime solution that dynamically tunes the rate of issuing hot and cold mini-

batches to ensure that the accuracy metrics are met.

Using these insights, we design a static-dynamic framework that not only reduces the overall training time but also minimizes the communication load and energy consumption. This framework ensures that the end-to-end training of recommender models do not incur any accuracy loss

III. DESIGN: THE FAE FRAMEWORK

This paper proposes the *Frequently Accessed Embeddings* (FAE) framework to accelerate training of recommender systems by efficiently utilizing the GPU memory capacity and computation throughput whilst reducing communication costs. Figure 5 illustrates the flow of the FAE framework for recommender models. The FAE framework consists of four components to efficiently capture and manage the hot embedding entries, replicating it across GPUs, while dynamically calibrating the accuracy and communication overheads.

The first component, called the *Calibrator* samples inputs and profiles them to understand the “hotness” of embedding entries. Based on allocated GPU memory size, confidence interval, and the CPU-GPU bandwidth, the Calibrator determines the access threshold to classify an embedding entry as hot. Based on this threshold, the second component *Input Processor* and *Embedding Classifier*, determines and categorizes embedding entries and sparse inputs into hot and cold portions, respectively. Hot inputs only access hot embedding entries whereas cold inputs can access any embedding entry. Both the Calibrator and classifiers execute statically, *once* per training dataset, and store the preprocessed data in a FAE format for subsequent training runs. The third component, called the *Embedding Replicator*, extracts *hot* embedding entries at runtime and creates embedding bags that are replicated across GPUs. The fourth component, called the *Shuffle Scheduler*, determines the execution order of hot and cold sparse input mini-batches at runtime for the CPU-GPU system. To meet the baseline accuracy goals, the Shuffle Scheduler interleaves the queuing of hot and cold mini-batches to capture the updates of embedding table entries from both these portions.

A. The Calibrator: Capacity vs Performance

The goal of calibrator is to pick an access threshold, which acts as knob to tradeoff hot embedding table size and performance, to categorize any training input as hot. As

discussed earlier, hot inputs can be executed in an accelerated data-parallel manner on GPUs. Picking a large access threshold would mean that only a very few embedding entries would have enough accesses to cross the threshold and be classified as hot. But this could help fit these hot embedding entries completely inside a GPU device memory. However, this would lead to only a small percentage of sparse-inputs to be categorized as hot and execute completely in a GPU execution mode, thus less performance benefits. Conversely, picking a small threshold will categorize embedding entries with very few accesses as hot and in turn would increase the embedding table size, often beyond the GPU device memory capacity. As shown in Figure 6, we observe diminishing returns by reducing the threshold, as the number of hot embedding entries increases more steeply as compared to hot inputs.

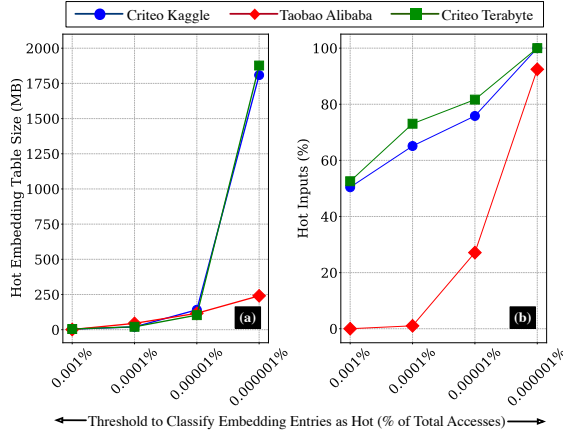


Fig. 6: (a) Size of hot embedding entries and (b) Percentage of hot sparse-inputs with varying access threshold values. As we vary the threshold, the size of the embedding entries increases more rapidly as compared to the percent of hot inputs.

Furthermore, as the threshold is decreased, the latency to preprocess sparse-inputs only increases as a larger set of inputs would now scan a greater amount of embedding table entries. One cannot naively reduce the access threshold. We need to intelligently tune the size of hot embeddings, size of hot inputs, and performance benefits.

To this end, the Calibrator, based on the system configuration such as input dataset size, embedding table sizes, and GPU memory capacity sets the access threshold for determining the hot embedding entries. A system can have several 100s of GBs of Dynamic Random Access Memory (DRAM) on CPU. For instance, while high-end CPUs like Intel-Xeon support up to 1TB DRAM capacity, even low-end CPUs like Intel-Core support up to 128GB DRAM capacity. In contrast, high-end GPU devices support only 10s of GBs of DRAM memory, for example high-end Nvidia Tesla-V100 supports a maximum of 32GB of DRAM. Therefore, it is vital for the Calibrator to ensure that the GPU memory is efficiently utilized.

To determine the access threshold, a naive Calibrator would have to profile the *entire* training dataset and analyze the access pattern of *all* the entries in *all* the embedding tables. This profiling phase requires sorting the access numbers of

all embedding entries, and only classifying the top h as hot, where h constitutes entries that fit within the allocated size. This rudimentary implementation can incur a high profiling overhead, even though it is only performed once per dataset, as it has to go through the whole dataset and all the entire embedding tables. Instead, the Calibrator employs the following statistical techniques to ensure a low static compilation overhead of finding the *final threshold*.

1) Mitigating Read Overheads with Sparse Input Sampler:

The sparse *input sampler* estimates the total accesses into embedding entries. As size of the training input dataset is typically very large and we sample $x\%$ of the total inputs (S_I). The value of x is specified as a hyper-parameter. For our implementation, we iterate through $x = 5\%$ of the entire dataset to obtain \hat{S}_I sampled sparse-inputs. Figure 7 shows the access profile for one large embedding table in the Kaggle, Terabyte, and Alibaba datasets with and without sparse input sampling. Empirically, we observe with 5% of the dataset, we can obtain the same access profile as the entire training data. Even with 5% sampling, we process $\geq 500K$ sparse inputs.

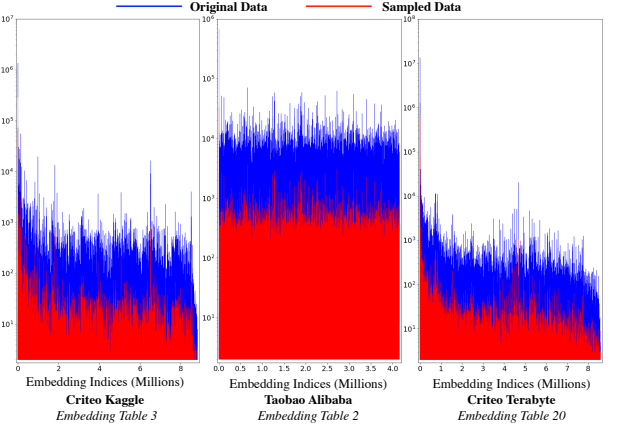


Fig. 7: The access profile into a large embedding table from the actual inputs and sampled inputs. The sample rate in this experiment is 5%. Randomly sampling even 5% of the dataset provides a similar access signature as the entire dataset.

The *profiler* then takes the output of the sparse input sampler (i.e. \hat{S}_I) and uses it to access large embedding tables (denoted by z). Our implementation assumes any embedding table that is greater than or equal to 1MB to be large. Embedding tables smaller than 1MB are de-facto considered to be “hot” as they can easily fit even on low-end GPU memories.

2) Tracking Accesses with Embedding Logger: The embedding logger keeps track of the number of accesses (k) into each entry for each embedding table (z) for the sampled inputs \hat{S}_I . This creates a sampled access profile for each embedding table entry. The key insight here is that as inputs are randomly sampled from the entire dataset, the access profile of the \hat{S}_I (sampled inputs) will closely track the S_I (total dataset). As shown in Figure 8, due to this sampling, we see $19\times$ to $55\times$ reduction in latency.¹

¹For Taobao Alibaba, each input consists of a stream of up to 21 sub-inputs and therefore, see a larger reduction in latency [27].

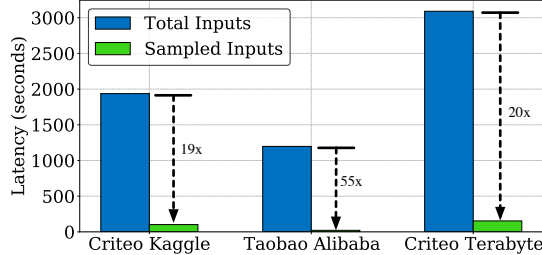


Fig. 8: Reduction in the profiling latency when input dataset is sampled for embedding table access pattern. The total time to sample decreases by $19\times$ to $55\times$, with a maximum time of only 200 seconds.

3) Converging on a Threshold using Statistical Optimizer:

The FAE framework uses a static value (L) on the amount of allocated GPU device memory that can be used by the hot-embedding table entries. The *Statistical Optimizer* repeatedly invokes its Rand-Em Box component, described below, with varying levels of access threshold with a desired confidence interval and converges on a final threshold.

Hot embedding size estimation using Rand-Em Box. The embedding logger creates a profile of accesses signatures for the sampled inputs. It still needs to estimate the hot embedding table sizes, *without* traversing all the embedding entries (10s of GBs). The *Rand-Em Box* uses the access threshold input from statistical optimizer and determines the estimated size of the hot-embedding entries *without* scanning entire embedding tables. To achieve this, the Rand-Em Box selects random samples of the embedding table entries. Typically, the sampled size is less than 1%-7% of the actual size of the embedding table. This enables the Calibrator to estimate the capacity overhead of hot embedding tables for a series of thresholds using a much smaller footprint of embedding entries.

Below, we provide the statistical evidence for using a sampler box on embedding entries to estimate the size of hot embedding tables for different thresholds. For an embedding z with N entries, each entry has k sparse-input accesses. Assuming an access threshold of t and the total number of sparse-inputs of S_I , we estimate the hot embedding cutoff, denoted by H_{zt} by using Equation 1:

$$H_{zt} = t \times S_I \quad (1)$$

We then pick n random samples from embedding table z . This paper uses the insight that one can use Central Limit Theorem (CLT) on the distribution of these samples and estimate the mean of the parent distribution. CLT has the property that, *irrespective of the parent distribution* (unknown in our case), the mean of the sampled distribution will always approach the mean of the parent distribution. Our implementation uses $n = 35$ and each sample consists of a chunk of m embedding table entries. This is because, when the sample size $n \geq 30$, CLT considers the sample size to be large and the sampled mean will be normal even if the sample does not originate from a Normal Distribution [37]. For higher precision, we use t-interval for our estimation. As each sample consists m of

1024 embedding entries we can estimate with a precision of $\frac{1}{1024}$ of the actual embedding table size. For each sample, we calculate the number of entries (k) greater than or equal to H_{zt} in the m -sized chunk. This is described by C and the total count of entries greater than or equal H_{zt} is represented by y . This is represented by Equation 2 and Equation 3:

$$C_{1..m} = \begin{cases} 1 & \text{if } k_{1..m} \geq H_{zt} \\ 0 & \text{otherwise} \end{cases} \quad (2)$$

$$y_t = \sum_{i=1}^m C_i \quad (3)$$

For sample values (n) which have a standard deviation of s , the sample mean, denoted by \bar{y}_t , is represented by Equation 4:

$$\bar{y}_t = \frac{\sum_{i=1}^n y_{ti}}{n} \quad (4)$$

As \bar{y} follows a t-distribution, the $100 \times (1-\alpha)$ confidence interval (CI) for \bar{y}_t is represented by Equation 5:

$$CI_{100 \times (1-\alpha)} = \bar{y}_t \pm t_{\frac{\alpha}{2}} \times \sqrt{\left(\frac{N-n}{N}\right) \times \left(\frac{s^2}{n}\right)} \quad (5)$$

For a 99.9% confidence and $n = 35$, the value of $t_{\frac{\alpha}{2}}$ is 3.340. Furthermore, large embedding tables tend to have $N \gg n$. Therefore, we can reduce Equation 5 to Equation 6:

$$CI_{99.9} = \bar{y}_t \pm 3.340 \times \frac{s}{\sqrt{35}} \quad (6)$$

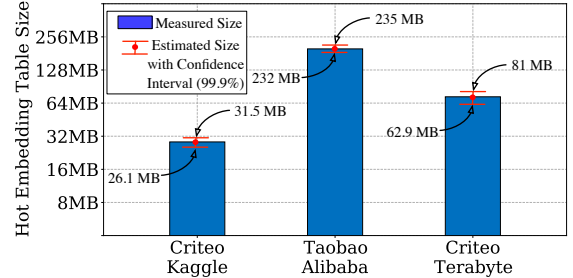


Fig. 9: Estimated sizes of hot embedding tables using random sampling with Rand-Em Box. For a confidence interval of 99.9%, the Rand-Em Box estimation is within 10% (upper bound) of the measured size.

The Rand-Em Box estimates the hot embedding table sizes for different access thresholds (t). For each estimation, the Rand-Em Box only needs to iterate on small number of sampled entries and does not scan the entire embedding table. Figure 9 shows the estimation of the Rand-Em Box estimation as compared to the actual values. The estimated values are within 10% of the measure values. For every threshold, the Rand-Em Box determines the size overhead of the hot embedding tables. Thereafter, based on the allocated GPU memory, either finalizes the threshold or adjusts it for the next iteration. GPU memory allocation for embedding (denoted by L) can be set by the user, our experiments show that $L = 256MB$ suffices and caters to all types of GPUs.

Figure 10 shows the latency savings from sampling embedding table. As the Statistical Optimizer scans at most 14x lower embedding entries for each iteration of t , the Rand-Em Box reduces latency by $14.5 \times 61 \times$.

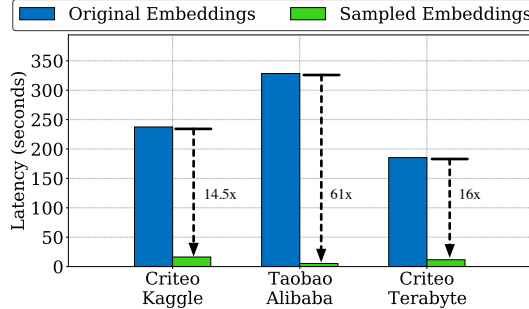


Fig. 10: Reduction in the *latency per iteration* by using Rand-Em Box to estimate the hot embedding size per threshold. We get $14.5 \times 61 \times$ lower latency. The *total* latency to scan all embedding tables is under 25 seconds per iteration.

The Statistical Optimizer then provides the final threshold its output to the next blocks in the FAE framework.

B. Embedding Classifier and Input Processor

The *embedding classifier* uses the output of the Embedding Logger and the Statistical Optimizer to tag all embedding table entries that meet the access threshold. This requires *only* one pass of each embedding table. During this pass, the Embedding Classifier generates a Hot-Embedding Bag that is sent to each GPU device during the training process.

Additionally, the *input processor* uses the final access threshold value from the Calibrator and accesses to the embedding table to identify hot sparse-inputs. Typically, there are 10s of embedding tables in a recommender model. A sparse-input typically accesses one or more entries in each of these embedding tables. A sparse-input is classified as hot only if all its embedding table accesses are to hot entries. This component typically requires only *one* pass of the entire sparse-input (S_I) and just checks if the embedding entry indices are present in the hot-embedding bags. As this is completely parallelizable operation across both inputs and embedding indices, we divide this task across multiple cores in the CPU. For a 16 core machine (32 hardware threads), the total time for this phase for different access thresholds is given by Figure 11.

The *input processor* is also responsible to bundle hot and cold inputs together into mini-batches. As aforementioned, we require the entire mini-batch to be hot to avoid the data shuffling between CPU and GPU. If one mini-batch of inputs is all hot, the entire execution can happen in a data-parallel mode on the GPU without any interference from the CPU. Once we have pre-processed the sparse-input data into hot and cold mini-batches, we store this in the FAE format for any subsequent training runs.

C. Input Scheduler: Dynamic Hot-Cold Swaps for Accuracy

All the profiling components in our FAE framework, i.e., Calibrator, Embedding Classifier, and Input Processor, provide

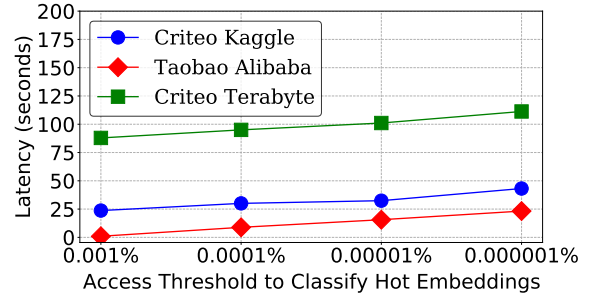


Fig. 11: The latency of the input processor to classify sparse-inputs (as hot or cold) as we vary the access threshold. Overall, even for very low access thresholds, we only require only a maximum of 110 seconds.

us with a dataset that is preprocessed into hot and cold mini-batches and a set of hot embeddings. The Embedding Replicator replicates the hot embedding bags across all GPUs, but a note here is that the hot embeddings also are available on CPU for baseline cold input executions. This is because cold inputs can access some hot embedding entries in some tables with simultaneously accessing cold embedding entries in other tables. Next, we discuss the runtime scheduling of hot and cold mini-batches to ensure baseline accuracy whilst providing accelerated performance.

Impact on accuracy. In the most basic form, FAE framework can schedule the entire collection of mini-batches comprising hot inputs followed by cold inputs, or vice versa, but such a schedule can have potential impacts on training accuracy. This is because the hot inputs only access and *update* the hot embedding entries, and training using only hot inputs for a long periods of time can potentially reduce the randomness in training. For non-convexity loss optimization problems, this makes gradient descent based algorithms susceptible to local minima [38, 39]. To mitigate this issue, machine learning community has often deployed data shuffling. Next, we discuss how we uniquely attenuate this issue for our framework.

Communication Overheads. To re-induce randomness in our training while also attaining accelerated performance, we can intermittently schedule hot and cold mini-batches. However, changing schedules of inputs very often can degrade performance as each of these events require synchronization of hot embedding parameters between CPU and GPU copies.

To balance this tradeoff of achieving accuracy but also obtaining performance, we offer Shuffle Scheduler that dynamically determines the interleaving of hot and cold inputs based on the runtime training metric. The scheduler always begins with training on cold inputs as they update a wider range of embedding entries, albeit infrequently per entry. The rate of scheduling hot and cold mini-batches can be tuned dynamically based on the following equation:

$$r(i+1) = \begin{cases} \min(r(i) * 1/2, R(1)) & \text{if } \Delta T_{stL}(i) \geq T_{stL}(i-1) \\ \max(r(i) * 2, R(100)) & \text{if } \Delta T_{stL}(i) \leq T_{stL}(i-u) \\ r(i) & \text{otherwise} \end{cases} \quad (7)$$

In the above equation, $r(i)$ is the rate at i^{th} swap. Rate of 100 ($R(100)$) implies that 100% of the mini-batches of cold

TABLE I: Model Architecture Parameters and Characteristics of the Datasets for our Workloads

| Workload | Dataset | Training Input | | Dataset Features | | Embedding Tables | | | Neural Network Config | | |
|-----------------|-----------------------|----------------|--------|------------------|--------|------------------|--------|-----------|-----------------------|---------------|-------------|
| | | Number | Size | Dense | Sparse | Number | Size | Dimension | Bottom MLP | Top MLP | DNN |
| RCM1 (TBSM [3]) | Taobao (Alibaba) [27] | 10 M | 1 GB | 3 | 16 | 3 | 0.3 GB | 4.1M×16 | 1-16 & 22-15-15 | 30-60-1 | Attn. Layer |
| RCM2 (DLRM [1]) | Criteo Kaggle [26] | 45 M | 2.5 GB | 13 | 16 | 26 | 2 GB | 10.1M×16 | 13-512-256-64-16 | 512-256-1 | - |
| RCM3 (DLRM [1]) | Criteo Terabyte [28] | 80 M | 45 GB | 13 | 64 | 26 | 61 GB | 73.1M×64 | 13-512-256-64 | 512-512-256-1 | - |

inputs will be completed before hot mini-batches are issued. A rate of $(R(1))$ implies hot and cold are scheduled after every mini-batch. On the basis of the test or test set loss, obtained after each schedule, we determine whether the rate needs to be changed based on the following two conditions.

First, if the framework observes an increase in the test loss from the previous schedule, it immediately reduces the rate by half. This implies that the remaining mini-batches of hot and cold inputs will be split into an alternate of cold and hot schedules. The rate can be reduced to a minimum of $R(1)$.

If the test loss decreases, rate is not changed, as this is the expected behaviour, unless the loss has been decreasing successively for u schedules. This is the second case where rate is changed, i.e., increased by 2 up to a max of $R(100)$. Like prior past work that offer automatic convergence checks to avoid overfitting, the downward trend of test loss curve [40] consecutively for 4 strips shows a balance between redundancy, badness, and slowness; thus we choose u as 4. Apart from the above two cases, the rate remains unchanged. This ensures that accuracy remains as the priority for the FAE framework. FAE always begins with $R(50)$ (alternate cold and hot mini-batches) for a dataset, and tunes the rate accordingly.

IV. EVALUATION

A. Experimental Setup

1) *Benchmarks and real-life datasets:* We showcase the efficacy of our FAE framework on 3 real world datasets, using common recommendation models RMC1, RMC2, and RMC3 which represent three classes of at-scale models [10]. We use open source implementation of Deep Learning Recommendation System (DLRM) [1] and Time-based Sequence Model for Personalization and Recommendation Systems (TBSM) [3] frameworks to train the above mentioned models. Based on the sparse input configuration, these datasets are used to train RMC1 model on Taobao Alibaba [27] with TBSM, RMC2 on Criteo Kaggle [26] with DLRM, and RMC3 on Criteo Terabyte [28] also with DLRM. Table I describes the details of the model architecture for RMC1, RMC2, and RMC3 including their dense and sparse features, embedding table numbers and size, and neural network configurations. TBSM architecture is built on DLRM and includes embedding layers, Bottom MLPs, and Top MLPs, like the latter, in addition to a deep learning attention layer. Table I also highlights the diversity of the model architectures in terms of embedding table sizes and neural network configurations.

For the first benchmark, which uses Taobao Alibaba dataset the goal is to predict user behavior. For the second benchmark, we use the publicly available Criteo Kaggle as dataset. Kaggle has a wide application in advertising to capture user's preference by predicting click-through rate. The third benchmark

trains on Criteo Terabyte dataset which provides the click logs of the users. In this paper we aim to cover recommender models meant to represent production-scale systems. As we do not have access to production-scale industry models, we rely on established open source recommender models such as DLRM and TBSM while using real-world datasets.

2) *Software libraries and setup:* DLRM and TBSM are configured using the Pytorch-1.7 and executed using Python-3. With Pytorch, we use the torch.distributed backend to support scalable distributed training and performance optimization [41]. For all the backend GPU to GPU communication, NCCL is used [42]. The baseline and FAE framework executions use gather, scatter, and all-reduce collective calls by using the backend NVLink [31].

3) *Server Architecture:* Table II describes the configuration of our datacenter servers.

TABLE II: System Specifications

| Device | Architecture | Memory | Storage |
|--------|---------------------------------|-------------------------|-----------------|
| CPU | Intel Xeon Silver 4116 (2.1GHz) | 768GB DDR4 (2.7GB/s) | 1.9 TB NVMe SSD |
| GPU | Nvidia Tesla V100 (1.2GHz) | 16 GB HBM-2.0 (900GB/s) | - |

These servers comprise 24-core Intel Xeon Silver 4116 (2.1 GHz) processor with Skylake architecture. Each server has a DRAM memory capacity of 192GB. Each DDR4-2666 channel has 8 GB memory. Each server also has a local storage of 1.9 TB NVMe SSD. Each server offers 4 NVIDIA Tesla-V100 each with 16GB memory capacity as a general purpose GPU. The GPUs are connected using the high speed NVLink-2.0 interconnect. Every GPU is communicating with the rest of the system via a 16x PCIe Gen3 bus. In this paper, we perform experiments on a single server with a maximum of 4 GPUs, as the open-sourced DLRM and TBSM models do not support multi-server implementations [1, 3]. However, even in a multi-server scenario, we expect our insights to hold true.

B. Results and Insights

1) *Accuracy Results:* Figure 12 illustrates the accuracy of Criteo Kaggle, Criteo Terabyte, and Taobao dataset for their RMC2, RMC3, and RMC1 models. The baseline here is the execution mode where embeddings execute on CPU and the MLP and DNN layers execute on GPUs, the baseline remains the same across Section IV-B. Table III shows the final convergence accuracy for all the workloads using a 4 GPU system. For the Criteo datasets, we use the testing accuracy and for the Taobao dataset we use the validation accuracy as established by previous baselines [3]. In the case of Criteo Kaggle and Taobao dataset, we observe that when the Shuffle Scheduler alternately issues cold and hot mini-batches at $R(50)$, the datasets are able to achieve the baseline

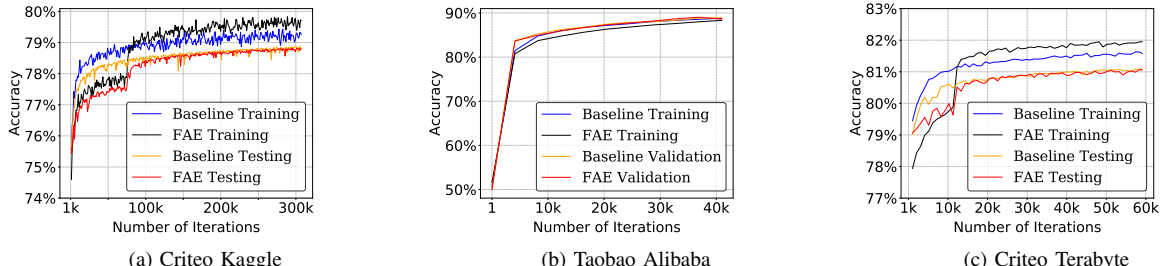


Fig. 12: Increasing Accuracy with training iterations when optimized with FAE framework. As we see, all the datasets and corresponding recommender models achieve the baseline accuracy for both training and test or validation sets.

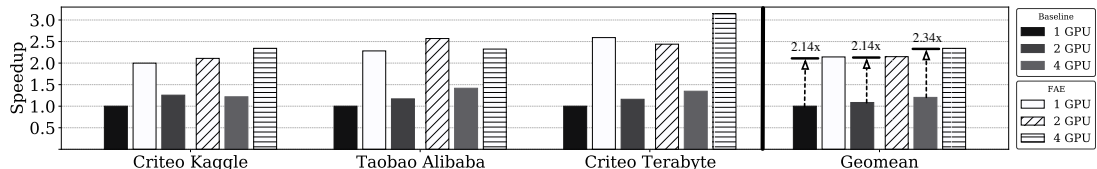


Fig. 13: The performance of Criteo Kaggle, Taobao Alibaba, and Criteo Terabyte training with the FAE framework vs a baseline where embedding layer is executed on the CPU and GPUs execute the neural network layers. All values are normalized to a system that uses 1 GPU. On average, the FAE framework provides up to 2.34x speedup across all three datasets.

accuracy. For the Criteo Terabyte dataset even a cold and hot input scheduling suffices and the optimized training achieves the baseline accuracy. We observe jumps in accuracy for both the Criteo datasets for the first time we switch from cold to hot inputs. This phenomenon can be attributed to the fact that initial cold mini-batches only update a very few embedding entries. But once we interleave it with the first mini-batch all the embedding entries get updated and we reach in the baseline accuracy for both training and testing sets.

TABLE III: Accuracy Comparison

| Dataset | Baseline Training (%) | FAE Training (%) | Baseline Testing (%) | FAE Testing (%) |
|-----------------|-----------------------|------------------|----------------------|-----------------|
| Criteo Kaggle | 79.30 | 79.70 | 78.86 | 78.86 |
| Taobao Alibaba | 88.78 | 88.32 | 89.21 | 89.03 |
| Criteo Terabyte | 81.62 | 81.95 | 81.07 | 81.06 |

2) *Training Time and Performance Improvements*: Figure 13 shows the performance improvement of training using FAE as compared to the baseline. The baseline is normalized to a 1 GPU system for each dataset. We use a mini-batch size of 1K, 256, and 1K for Criteo Kaggle, Taobao Alibaba, and Criteo Terabyte, respectively. FAE reduces the average training time by 54%, 54%, and 58%, for 1 GPU, 2 GPU, and 4 GPU executions, respectively. These comparisons are when the number of devices remain same for baseline and FAE. We maintain weak scaling across distributed runs where the mini-batch size is scaled with the number of GPUs. For example, the 2 GPU execution uses 2K, 512, and 2K mini-batch size for Criteo Kaggle, Taobao Alibaba, and Criteo Terabyte, respectively. The 4 GPU execution benefits the most because as the number of GPUs increase, the CPU-GPU communication overhead increases, and FAE eliminates this for hot inputs. For Taobao, 4 GPU executions takes more time than 2 GPU executions because the dataset is relatively small, thus the cold mini-batch executions overshadow our benefits. The FAE optimized training tends to outperforms the baseline.

Table IV shows training time for minibatch size of 1k, 2k, and 4k for Criteo Kaggle and Terabyte and 256, 512 and 1k for Taobao Alibaba dataset, respectively.

TABLE IV: Absolute Training Time – 10 Epochs (mins)

| Dataset | 1 GPU | | 2 GPUs | | 4 GPUs | |
|-----------------|----------|-------|----------|-------|----------|-------|
| | Baseline | FAE | Baseline | FAE | Baseline | FAE |
| Criteo Kaggle | 245.3 | 122.7 | 195.2 | 116.2 | 201.3 | 104.7 |
| Taobao Alibaba | 996.5 | 436.5 | 851.8 | 387.8 | 703.3 | 428.5 |
| Criteo Terabyte | 491.7 | 189.7 | 423.6 | 201.6 | 364.8 | 156.4 |

3) *Latency breakdown*.: Figure 14 shows the breakdown of the total runtime for each of the workloads executing on 1, 2, and 4 GPUs. We employ a weak scaling technique where 1 GPU execution uses 1024, 256, and 1024 mini-batch size for Criteo Kaggle, Taobao Alibaba, and Criteo Terabyte datasets, respectively. This mini-batch size is scaled as the number of devices increase. In Figure 14, the colors for cold inputs are consistent across baseline and FAE executions as they both execute in hybrid CPU-GPU mode.

Figure 14 shows that the optimizer time is a large portion of the baseline execution. This is because, after the backward pass, the gradients are transferred from the GPUs into the CPU and the optimizer is executed on the CPU for the embedding layers. The optimizer, such as Stochastic Gradient Descent, is massively parallel and therefore is not well suited for CPU execution. FAE is able to mitigate some of these inefficiencies and reduce the optimizer time for the hot input mini-batches. Hence, for FAE training the optimizer portion for the hot mini-batches is significantly lower than the cold mini-batches, even though the size of hot inputs is much higher than cold inputs.

One overhead imposed by the FAE framework is the embedding synchronization while switching between cold and hot mini-batches. This overhead is shown by the embedding sync portion on FAE executions. Both Criteo Kaggle and Criteo Terabyte use DLRM system, but the Kaggle has a higher percentage of embedding synchronization overhead because of its larger hot embedding size. On the contrary, Taobao dataset executing on TBSM observes the least percentage of synchronization overhead. This can be attributed to the high percent of forward and backward time of the Taobao

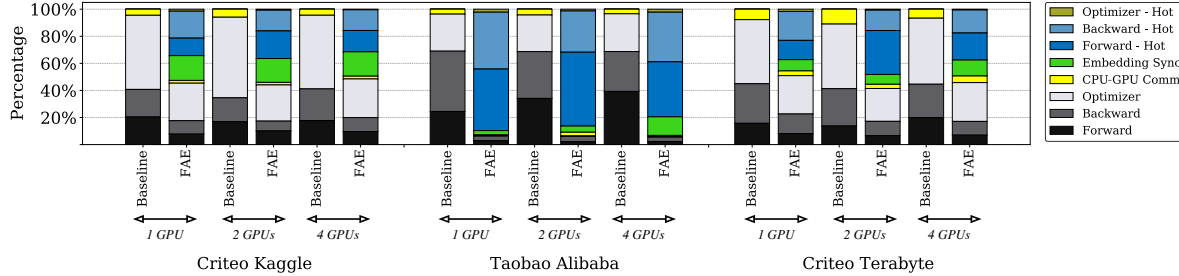


Fig. 14: Latency breakdown for the 1, 2, and 4 GPU executions. The FAE framework adds the overhead of embedding synchronization across CPUs and GPUs, not present in baseline. However, FAE eliminates the slow CPU optimization execution for hot mini-batches.

RMCI recommender model due to its deep attention layer. Thus, as the recommender models become bigger with larger embedding tables and deeper neural network layers, FAE can offer higher benefits by reducing the CPU-GPU data transfer between embedding and DNN layers (which also increases with DNN size), and also observe amortized embedding synchronization overheads. Even though embedding tables are expected to increase in size, a larger absolute size of embedding table does not imply a proportionally large hot embedding table. This is because certain inputs are always going to be more popular than the others.

CPU-GPU Transfer Overheads Figure 14 shows the percentage of time spent on transferring embedding layer from CPU to GPU. Additionally, Table V shows the absolute communication time to transfer the embedding layers.

TABLE V: CPU-GPU Communication – 10 Epochs (mins)

| Dataset | 1 GPU | | 2 GPUs | | 4 GPUs | |
|-----------------|----------|------|----------|-------|----------|------|
| | Baseline | FAE | Baseline | FAE | Baseline | FAE |
| Criteo Kaggle | 11.05 | 2.5 | 11.56 | 2.17 | 9.0 | 2.14 |
| Taobao Alibaba | 36.21 | 3.09 | 36.53 | 10.60 | 23.90 | 5.77 |
| Criteo Terabyte | 38.0 | 6.63 | 46.49 | 6.20 | 24.21 | 7.62 |

In the baseline, bigger Models with larger volume of embedding tables (Terabyte dataset) spend more time performing this transfer (both absolute time and percentage). This is because, even though larger models require more compute, compute can be disproportionately accelerated with GPUs whereas communication cannot be. FAE does not incur as large of this overhead with increasing model size as it eliminate the CPU-GPU communication entirely for hot inputs.

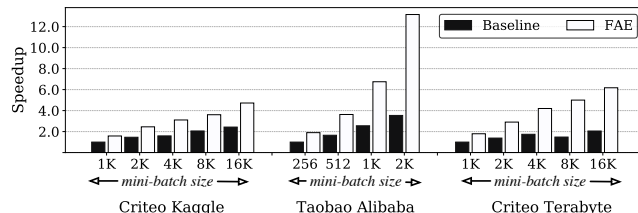


Fig. 15: Performance improvement of FAE optimized training with varying mini-batch sizes. FAE provides up to 4.7x speedup for large mini-batch sizes.

4) Performance improvement with varying mini-batch size: Figure 15 shows the performance benefits of FAE optimized training over the baseline execution. In this graph, 1-GPU execution is the uniform baseline. As the mini-batch size increases, we observe higher benefits because the overheads of FAE framework are amortized over a large input set. For instance, now the Embedding Replicator replicates the model fewer times. However, for the baseline the improvements come because of the reduced number of times optimizer is being executed in CPU, which is anyway an improvement for FAE for its cold mini-batches.

5) Power Benefits: Table VI shows the per GPU power consumption using the baseline and the FAE framework for a 1024 mini-batch.

TABLE VI: GPU Power Consumption Comparison

| Dataset | Baseline | FAE | Reduction |
|-----------------|----------|--------|-----------|
| Criteo Kaggle | 58.91W | 55.81W | 5.3% |
| Alibaba | 60.21W | 56.62W | 6% |
| Criteo Terabyte | 62.47W | 57.03W | 8.8% |

We see a reduction in the total power consumption across all datasets. This enables FAE framework to reduce GPU power by 5.3% to 8.8%. This is primarily because of the reduced communication costs between devices.

V. RELATED WORK

Training of machine learning models is an important and heavily developed area of research. The focus in this area has mainly been on optimizing deep neural networks training [6, 13, 30, 43, 44]. Instead in this work we focus on optimizing training of recommender system models. Prior work on recommender models with industry-scale datasets show that access patterns follow a Power or Zipfian distribution [45] and thereby reaffirm our observation on hot embedding entries.

Mixed-precision training for Recommender Models. Prior work [46], optimizes training by modifying the model either through mixed-precision training or eliminating rare categorical variables to reduce the embedding table size. Even with these optimizations real dataset's entire embedding table cannot fit on a GPU. Such approaches that change the data representation and/or embedding tables, require accuracy re-validation across a variety of models and datasets. FAE on the other hand performs full-precision training of the baseline

model by leveraging the highly skewed access pattern for embedded tables and increase the throughput for hot embedding entries. Nevertheless, we quantitatively compared NvOPT with FAE. Overall, **FAE is 1.48x faster than NvOPT** for the TeraByte Dataset. FAE reduces the per epoch training time from 105.98 mins to 71.58 mins (mini-batch size of 32K) on single V100 GPU as the most frequently access embedding tables are placed on the GPU memory.

Embedding Parameter Placement. Works in [47] offers a hierarchical parameter server that builds a distributed hash table across multiple GPUs. This work stores the working parameters close to computation, i.e, GPU, at runtime, albeit treats all embedding entries equally. Instead, FAE delves into the access pattern of each dataset and uses this information to store the highly accessed embedding entries in the GPU for the entirety of the training job. Work in [48], aims to understand the implications of different embedding table placements within an heterogeneous data-centre. However, none of the techniques leverage runtime access skew for their embedding table placement that can improve the overall training performance.

Recommendation models and designs. Recently, there has been interest in deep learning based recommender models that use embedding tables [49] augmented with deep learning algorithms [1, 3, 50] to incorporate relevant query features and item features to capture the specific interests of a user. However, unlike prior work in DNNs [36, 51–54] that focus on dense features, deep learning based recommendation models employ both sparse and dense features through embedding tables and neural networks, respectively. We focus on these types of models as they are commonly used at production levels and are responsible for large number of compute cycles in data centres [10, 55]. Even with their popularity, a lot of the research has focused on neural network optimizations for inference of these models [10, 19, 56–58]. However, the training process tends to be more intensive, both from the memory and the compute perspective. Certain solutions that offer training system optimizations [59, 60] and acceleration [7, 43, 61] either do not support deep learning based algorithms or do not offer distributed GPU based training schemes. Prior work like “Tensor casting” [18] define a tensor casting algorithm that transforms compute primitive for forward and backward propagation during the training. Instead, in this work we do not transform the compute portion of the training graph rather facilitate better memory and bandwidth utilization.

Distributed machine learning training. Distributed training has become the norm to train large scale models. Data parallel training [35] forms the most common form of distributed training as it only requires synchronization after the gradients generated in backward pass of training. However, as models become bigger and bigger [29, 62], model parallelism [44, 63] and pipeline parallelism [30] are becoming common as they split a single model onto multiple devices. Nevertheless, the techniques employed to automatically split the models [64, 65], offer model parallelism solutions to enable training of

large model with size constrained by the accelerator memory capacity. Unlike DNNs, for recommender models, even though embedding tables are becoming larger, splitting them across devices just for memory capacity (especially GPUs) is sub-optimal and does not effectively utilize GPU resources. In this work, in contrast to past model parallelism work of splitting model, we use the fact that embedding table does not have to be fully replicated to perform data parallel training, instead only hot embedding entries can be sent to all the devices. Nonetheless, our optimization is orthogonal to these past techniques, as it can be employed in tandem with pipeline and model parallel distributed training to reduce the memory footprint further of embedding table per device.

Optimizations to mitigate memory intensive training. Works in [66] propose techniques to store embedding tables in non-volatile memories and allocate a certain portion of DRAM for caching. This work, however, does not support GPU based training executions with replicated hot embeddings and does not deal with perceptive input pre-processing to reduce the overhead of communication. Recent work in [59–61] has also proposed solutions to accelerate near-memory processing for embedding tables, but do not facilitate distributed training using GPUs. More work has been done on compression [23–25] and sparsity [67] to reduce the memory footprint of machine learning models in general. We believe our framework obtains better memory utilization of devices without employing overheads such as compression/decompression and sparse operations. Nevertheless, our framework is orthogonal to these techniques and can be used in tandem with them to improve the memory efficiency even further.

VI. CONCLUSIONS

Recommendation models aim to learn user preferences by employing very large embedding tables that often cannot fit on GPUs. However, these models also comprise neural network layers that are very well suited for GPUs. These contrasting requirements splits the training execution on CPUs (for memory capacity) and GPUs (for compute throughput). Fortunately, for real-world data, we observe that embedding tables showcase a very skewed data access pattern. This is because, in the real world, certain training inputs (users and items) are often much more popular than the others. This observation allows us to develop a comprehensive framework, namely FAE, that uses statistical techniques to quantify the hotness of embedding entries based on the input dataset. This hotness of embedding tables in turn allows the framework to employ a GPU accelerated execution for inputs that only access these hot embedding entries. To capture most of the performance benefits the FAE bundles hot inputs and cold inputs in separate mini-batches. This helps FAE to reduce any CPU-GPU transfer overhead within a hot mini-batch. The training for these hot inputs happens entirely on GPUs, thus reducing any CPU-GPU communication overhead between CPU-GPU and GPU-GPU from embedding and neural network layers. Overall, the FAE, on average, speeds-up the training process for state-of-the-art models by 2.34 \times .

REFERENCES

[1] Maxim Naumov, Dheevatsa Mudigere, Hao-Jun Michael Shi, Jianyu Huang, Narayanan Sundaraman, Jongsoo Park, Xiaodong Wang, Udit Gupta, Carole-Jean Wu, Alisson G. Azzolini, Dmytro Dzhulgakov, Andrey Mallevich, Ilia Cherniavskii, Yinghai Lu, Raghuraman Krishnamoorthi, Ansha Yu, Volodymyr Kondratenko, Stephanie Pereira, Xianjie Chen, Wenlin Chen, Vijay Rao, Bill Jia, Liang Xiong, and Misha Smelyanskiy. Deep learning recommendation model for personalization and recommendation systems. *CoRR*, abs/1906.00091, 2019. URL <https://arxiv.org/abs/1906.00091>.

[2] Xiangnan He, Lizi Liao, Hanwang Zhang, Liqiang Nie, Xia Hu, and Tat-Seng Chua. Neural collaborative filtering. In *Proceedings of the 26th International Conference on World Wide Web, WWW '17*, page 173–182, Republic and Canton of Geneva, CHE, 2017. International World Wide Web Conferences Steering Committee. ISBN 9781450349130. doi: 10.1145/3038912.3052569. URL <https://doi.org/10.1145/3038912.3052569>.

[3] T. Ishkhanov, M. Naumov, X. Chen, Y. Zhu, Y. Zhong, A. G. Azzolini, C. Sun, F. Jiang, A. Malevich, and L. Xiong. Time-based sequence model for personalization and recommendation systems. *CoRR*, abs/2008.11922, 2020. URL <https://arxiv.org/abs/2008.11922>.

[4] Norman P. Jouppi, Cliff Young, Nishant Patil, David Patterson, Gaurav Agrawal, Raminder Bajwa, Sarah Bates, Suresh Bhatia, Nan Boden, Al Borchers, Rick Boyle, Pierre-luc Cantin, Clifford Chao, Chris Clark, Jeremy Coriell, Mike Daley, Matt Dau, Jeffrey Dean, Ben Gelb, Tara Vazir Ghaemmaghami, Rajendra Gotipati, William Gulland, Robert Hagmann, C. Richard Ho, Doug Hogberg, John Hu, Robert Hundt, Dan Hurt, Julian Ibarz, Aaron Jaffey, Alek Jaworski, Alexander Kaplan, Harshit Khaitan, Daniel Killebrew, Andy Koch, Naveen Kumar, Steve Lacy, James Laudon, James Law, Diemthu Le, Chris Leary, Zhuyuan Liu, Kyle Lucke, Alan Lundin, Gordon MacKean, Adriana Maggiore, Maire Mahony, Kieran Miller, Rahul Nagarajan, Ravi Narayanaswami, Ray Ni, Kathy Nix, Thomas Norrie, Mark Omernick, Narayana Penukonda, Andy Phelps, Jonathan Ross, Matt Ross, Amir Salek, Emad Samadiani, Chris Severn, Gregory Sizikov, Matthew Snelham, Jed Souter, Dan Steinberg, Andy Swing, Mercedes Tan, Gregory Thorson, Bo Tian, Horia Toma, Erick Tuttle, Vijay Vasudevan, Richard Walter, Walter Wang, Eric Wilcox, and Doe Hyun Yoon. In-datacenter performance analysis of a tensor processing unit. In *Proceedings of the 44th Annual International Symposium on Computer Architecture, ISCA '17*, page 1–12, New York, NY, USA, 2017. Association for Computing Machinery. ISBN 9781450348928. doi: 10.1145/3079856.3080246. URL <https://doi.org/10.1145/3079856.3080246>.

[5] Eric Chung, Jeremy Fowers, Kalin Ovtcharov, , Adrian Caulfield, Todd Massengill, Ming Liu, Mahdi Ghandi, Daniel Lo, Steve Reinhardt, Shlomi Alkalay, Hari Angepat, Derek Chiou, Alessandro Forin, Doug Burger, Lisa Woods, Gabriel Weisz, Michael Haselman, and Dan Zhang. Serving dnns in real time at datacenter scale with project brainwave. *IEEE Micro*, 38:8–20, March 2018. URL <https://www.microsoft.com/en-us/research/publication/serving-dnns-real-time-datacenter-scale-project-brainwave/>.

[6] Yunji Chen, Tao Luo, Shaoli Liu, Shijin Zhang, Liqiang He, Jia Wang, Ling Li, Tianshi Chen, Zhiwei Xu, Ninghui Sun, et al. Dadiannao: A machine-learning supercomputer. In *MICRO*, 2014.

[7] Divya Mahajan, Jongse Park, Emmanuel Amaro, Hardik Sharma, Amir Yazdanbakhsh, Joon Kim, and Hadi Esmaeilzadeh. TABLA: A unified template-based framework for accelerating statistical machine learning. March 2016.

[8] Yu-Hsin Chen, Joel Emer, and Vivienne Sze. Eyeriss: A Spatial Architecture for Energy-Efficient Dataflow for Convolutional Neural Networks. In *ISCA*, 2016.

[9] Carlos A. Gomez-Uribe and Neil Hunt. The netflix recommender system: Algorithms, business value, and innovation. *ACM Trans. Manage. Inf. Syst.*, 6(4), December 2016. ISSN 2158-656X. doi: 10.1145/2843948. URL <https://doi.org/10.1145/2843948>.

[10] U. Gupta, C. Wu, X. Wang, M. Naumov, B. Reagen, D. Brooks, B. Cottel, K. Hazelwood, M. Hempstead, B. Jia, H. S. Lee, A. Malevich, D. Mudigere, M. Smelyanskiy, L. Xiong, and X. Zhang. The architectural implications of facebook’s dnn-based personalized recommendation. In *2020 IEEE International Symposium on High Performance Computer Architecture (HPCA)*, pages 488–501, 2020. doi: 10.1109/HPCA47549.2020.00047.

[11] B. Smith and G. Linden. Two decades of recommender systems at amazon.com. *IEEE Internet Computing*, 21(3):12–18, 2017. doi: 10.1109/MIC.2017.72.

[12] Jeffrey Dean, Greg Corrado, Rajat Monga, Kai Chen, Matthieu Devin, Mark Mao, Marc’ aurelio Ranzato, Andrew Senior, Paul Tucker, Ke Yang, Quoc Le, and Andrew Ng. Large scale distributed deep networks. In F. Pereira, C. J. C. Burges, L. Bottou, and K. Q. Weinberger, editors, *Advances in Neural Information Processing Systems*, volume 25, pages 1223–1231. Curran Associates, Inc., 2012. URL <https://proceedings.neurips.cc/paper/2012/file/6aca97005c68f1206823815f66102863-Paper.pdf>.

[13] Myeongjae Jeon, Shivaram Venkataraman, Amar Phanishayee, unjie Qian, Wencong Xiao, and Fan Yang. Analysis of large-scale multi-tenant gpu clusters for dnn training workloads. In *Proceedings of the 2019 USENIX Conference on Usenix Annual Technical Conference, USENIX ATC ’19*, page 947–960, USA, 2019. USENIX Association. ISBN 9781939133038.

[14] Abhinandan Majumdar, Srihari Cadambi, Michela Be-

chi, Srimat T. Chakradhar, and Hans Peter Graf. A massively parallel, energy efficient programmable accelerator for learning and classification. *ACM Trans. Archit. Code Optim.*, 9(1):6:1–6:30, March 2012. ISSN 1544-3566. doi: 10.1145/2133382.2133388. URL <http://doi.acm.org/10.1145/2133382.2133388>.

[15] Maxim Naumov, John Kim, Dheevatsa Mudigere, Srinivas Sridharan, Xiaodong Wang, Whitney Zhao, Serhat Yilmaz, Changkyu Kim, Hector Yuen, Mustafa Ozdal, Krishnakumar Nair, Isabel Gao, Bor-Yiing Su, Jiyan Yang, and Mikhail Smelyanskiy. Deep Learning Training in Facebook Data Centers: Design of Scale-up and Scale-out Systems. *arXiv e-prints*, art. arXiv:2003.09518, March 2020.

[16] Jianyu Huang, Jongsoo Park, Ping Tak Peter Tang, Andrew Tulloch, et al. Mixed-precision embedding using a cache. *arXiv preprint arXiv:2010.11305*, 2020.

[17] Weijie Zhao, Jingyuan Zhang, Deping Xie, Yulei Qian, Ronglai Jia, and Ping Li. Aibox: Ctr prediction model training on a single node. In *Proceedings of the 28th ACM International Conference on Information and Knowledge Management*, pages 319–328, 2019.

[18] Youngeun Kwon, Yunjae Lee, and Minsoo Rhu. Tensor casting: Co-designing algorithm-architecture for personalized recommendation training. *arXiv preprint arXiv:2010.13100*, 2020.

[19] Youngeun Kwon, Yunjae Lee, and Minsoo Rhu. Tensor-dimm: A practical near-memory processing architecture for embeddings and tensor operations in deep learning. In *Proceedings of the 52nd Annual IEEE/ACM International Symposium on Microarchitecture*, pages 740–753, 2019.

[20] Itay Hubara, Matthieu Courbariaux, Daniel Soudry, Ran El-Yaniv, and Yoshua Bengio. Binarized neural networks. In *Proceedings of the 30th International Conference on Neural Information Processing Systems*, NIPS’16, page 4114–4122, Red Hook, NY, USA, 2016. Curran Associates Inc. ISBN 9781510838819.

[21] Suyog Gupta, Ankur Agrawal, Kailash Gopalakrishnan, and Pritish Narayanan. Deep learning with limited numerical precision. In *Proceedings of the 32nd International Conference on International Conference on Machine Learning - Volume 37*, ICML’15, page 1737–1746. JMLR.org, 2015.

[22] Song Han, Huizi Mao, and William J Dally. Deep compression: Compressing deep neural networks with pruning, trained quantization and huffman coding. *arXiv preprint arXiv:1510.00149*, 2015.

[23] A. Jain, A. Phanishayee, J. Mars, L. Tang, and G. Pekhimenko. Gist: Efficient data encoding for deep neural network training. In *2018 ACM/IEEE 45th Annual International Symposium on Computer Architecture (ISCA)*, pages 776–789, 2018. doi: 10.1109/ISCA.2018.00070.

[24] Yang Sun, Fajie Yuan, Min Yang, Guoao Wei, Zhou Zhao, and Duo Liu. A generic network compression framework for sequential recommender systems. In *Proceedings of the 43rd International ACM SIGIR Conference on Research and Development in Information Retrieval*, SIGIR ’20, page 1299–1308, New York, NY, USA, 2020. Association for Computing Machinery. ISBN 9781450380164. doi: 10.1145/3397271.3401125. URL <https://doi.org/10.1145/3397271.3401125>.

[25] Xiaorui Wu, Hong Xu, Honglin Zhang, Huaming Chen, and Jian Wang. Saec: similarity-aware embedding compression in recommendation systems. In *Proceedings of the 11th ACM SIGOPS Asia-Pacific Workshop on Systems*, pages 82–89, 2020.

[26] CriteoLabs. Criteo display ad challenge, . <https://www.kaggle.com/c/criteo-display-ad-challenge>.

[27] Alibaba. User behavior data from taobao for recommendation. <https://tianchi.aliyun.com/dataset/dataDetail?dataId=649&userId=1>.

[28] CriteoLabs. Terabyte click logs, . <https://labs.criteo.com/2013/12/download-terabyte-click-logs>.

[29] C Rosset. Turing-nlg: A 17-billion-parameter language model by microsoft. *Microsoft Blog*, 2019.

[30] Deepak Narayanan, Aaron Harlap, Amar Phanishayee, Vivek Seshadri, Nikhil R. Devanur, Gregory R. Ganger, Phillip B. Gibbons, and Matei Zaharia. Pipedream: Generalized pipeline parallelism for dnn training. In *Proceedings of the 27th ACM Symposium on Operating Systems Principles*, SOSP ’19, page 1–15, New York, NY, USA, 2019. Association for Computing Machinery. ISBN 9781450368735. doi: 10.1145/3341301.3359646. URL <https://doi.org/10.1145/3341301.3359646>.

[31] Nvlink. URL <https://developer.nvidia.com/nccl>.

[32] Guanhua Wang, S. Venkataraman, Amar Phanishayee, Jorgen Thelin, Nikhil R. Devanur, and I. Stoica. Blink: Fast and generic collectives for distributed ml. *ArXiv*, abs/1910.04940, 2020.

[33] K. Cho, M. Lee, K. Park, T. T. Kwon, Y. Choi, and Sangheon Park. Wave: Popularity-based and collaborative in-network caching for content-oriented networks. In *2012 Proceedings IEEE INFOCOM Workshops*, pages 316–321, 2012. doi: 10.1109/INFCOMW.2012.6193512.

[34] Fragkiskos Papadopoulos, Maksim Kitsak, M. A. Serrano, Marian Boguna, and Dmitri Krioukov. Popularity versus similarity in growing networks. *Nature*, 489(7417):537–40, Sep 27 2012. URL <https://ezproxy.library.ubc.ca/login?url=https://www-proquest-com.ezproxy.library.ubc.ca/docview/1095114119?accountid=14656>. Copyright - Copyright Nature Publishing Group Sep 27, 2012; Document feature - Illustrations; Graphs; ; Last updated - 2019-09-06; CODEN - NATUAS.

[35] Alex Krizhevsky, Ilya Sutskever, and Geoffrey E. Hinton. Imagenet classification with deep convolutional neural networks. *Commun. ACM*, 60(6):84–90, May 2017. ISSN 0001-0782. doi: 10.1145/3065386. URL <https://doi.org/10.1145/3065386>.

[36] Jacob Devlin, Ming-Wei Chang, Kenton Lee, and Kristina Toutanova. Bert: Pre-training of deep bidirectional transformers for language understanding. *arXiv*

preprint arXiv:1810.04805, 2018.

- [37] Runger Montgomery. Applied statistics and probability for engineers.
- [38] B. Recht and C. Ré. Parallel stochastic gradient algorithms for large-scale matrix completion. *Mathematical Programming Computation*, 5:201–226, 2013.
- [39] Léon Bottou. Stochastic gradient descent tricks. In *Neural networks: Tricks of the trade*, pages 421–436. Springer, 2012.
- [40] Lutz Prechelt. Early stopping-but when? In *Neural Networks: Tricks of the trade*, pages 55–69. Springer, 1998.
- [41] Adam Paszke, Sam Gross, Soumith Chintala, Gregory Chanan, Edward Yang, Zachary DeVito, Zeming Lin, Alban Desmaison, Luca Antiga, and Adam Lerer. Automatic differentiation in pytorch. 2017.
- [42] Nvidia. NVIDIA Collective Communications Library (NCCL). <https://docs.nvidia.com/deeplearning/nccl/index.html>.
- [43] Jongse Park, Hardik Sharma, Divya Mahajan, Joon Kyung Kim, Preston Olds, and Hadi Esmaeilzadeh. Scale-out acceleration for machine learning. October 2017.
- [44] Yanping Huang, Youlong Cheng, Ankur Bapna, Orhan Firat, Dehao Chen, Mia Xu Chen, HyoukJoong Lee, Jiquan Ngiam, Quoc V. Le, Yonghui Wu, and Zhifeng Chen. Gpipe: Efficient training of giant neural networks using pipeline parallelism. In Hanna M. Wallach, Hugo Larochelle, Alina Beygelzimer, Florence d’Alché-Buc, Emily B. Fox, and Roman Garnett, editors, *Advances in Neural Information Processing Systems 32: Annual Conference on Neural Information Processing Systems 2019, NeurIPS 2019, 8-14 December 2019, Vancouver, BC, Canada*, pages 103–112, 2019. URL <http://papers.nips.cc/paper/8305-gpipe-efficient-training-of-giant-neural-networks-using-pipeline-parallelism>.
- [45] Chunxing Yin, Bilge Acun, Xing Liu, and Carole-Jean Wu. Tt-rec: Tensor train compression for deep learning recommendation models, 2021.
- [46] Mengdi Huang Nvidia Inc. Vinh Nguyen, Tomasz Grel. Optimizing the deep learning recommendation model on nvidia gpus. <https://developer.nvidia.com/blog/optimizing-dlrm-on-nvidia-gpus>.
- [47] Weijie Zhao, Deping Xie, Ronglai Jia, Yulei Qian, Ruiquan Ding, Mingming Sun, and Ping Li. Distributed hierarchical gpu parameter server for massive scale deep learning ads systems, 2020.
- [48] Bilge Acun, Matthew Murphy, Xiaodong Wang, Jade Nie, Carole-Jean Wu, and Kim Hazelwood. Understanding training efficiency of deep learning recommendation models at scale, 2020.
- [49] Jui-Ting Huang, Ashish Sharma, Shuying Sun, Li Xia, David Zhang, Philip Pronin, Janani Padmanabhan, Giuseppe Ottaviano, and Linjun Yang. *Embedding-Based Retrieval in Facebook Search*, page 2553–2561. Association for Computing Machinery, New York, NY, USA, 2018. ISBN 9781450379984. URL <https://doi.org/10.1145/3394486.3403059>.
- [50] Shuai Zhang, Lina Yao, Aixin Sun, and Yi Tay. Deep learning based recommender system: A survey and new perspectives. *ACM Comput. Surv.*, 52(1), February 2019. ISSN 0360-0300. doi: 10.1145/3285029. URL <https://doi.org/10.1145/3285029>.
- [51] Alex Krizhevsky, Ilya Sutskever, and Geoffrey E Hinton. Imagenet classification with deep convolutional neural networks. *Communications of the ACM*, 60(6):84–90, 2017.
- [52] Christian Szegedy, Alexander Toshev, and Dumitru Erhan. Deep neural networks for object detection. In *Advances in neural information processing systems*, pages 2553–2561, 2013.
- [53] Sepp Hochreiter and Jürgen Schmidhuber. Long short-term memory. *Neural computation*, 9(8):1735–1780, 1997.
- [54] Ashish Vaswani, Noam Shazeer, Niki Parmar, Jakob Uszkoreit, Llion Jones, Aidan N. Gomez, Ł. Kaiser, and Illia Polosukhin. Attention is all you need. In *NIPS*, 2017.
- [55] Maxim Naumov, John Kim, Dheevatsa Mudigere, Srinivas Sridharan, Xiaodong Wang, Whitney Zhao, Serhat Yilmaz, Changkyu Kim, Hector Yuen, Mustafa Ozdal, et al. Deep learning training in facebook data centers: Design of scale-up and scale-out systems. *arXiv preprint arXiv:2003.09518*, 2020.
- [56] Ranggi Hwang, Taehun Kim, Youngeun Kwon, and Minsoo Rhu. Centaur: A chiplet-based, hybrid sparse-dense accelerator for personalized recommendations. *arXiv preprint arXiv:2005.05968*, 2020.
- [57] Udit Gupta, Samuel Hsia, Vikram Saraph, Xiaodong Wang, Brandon Reagen, Gu-Yeon Wei, Hsien-Hsin S Lee, David Brooks, and Carole-Jean Wu. Deeprecsys: A system for optimizing end-to-end at-scale neural recommendation inference. *arXiv preprint arXiv:2001.02772*, 2020.
- [58] Nvidia. Accelerating wide deep recommender inference on gpus, 2017. <https://developer.nvidia.com/blog/accelerating-wide-deep-recommender-inference-on-gpus/>.
- [59] A. Ginart, M. Naumov, D. Mudigere, Jiyan Yang, and J. Zou. Mixed dimension embeddings with application to memory-efficient recommendation systems. *ArXiv*, abs/1909.11810, 2019.
- [60] Hao-Jun Michael Shi, Dheevatsa Mudigere, Maxim Naumov, and Jiyan Yang. *Compositional Embeddings Using Complementary Partitions for Memory-Efficient Recommendation Systems*, page 165–175. Association for Computing Machinery, New York, NY, USA, 2020. ISBN 9781450379984. URL <https://doi.org/10.1145/3394486.3403059>.
- [61] L. Ke, U. Gupta, B. Y. Cho, D. Brooks, V. Chandra, U. Diril, A. Firoozshahian, K. Hazelwood, B. Jia, H. S. Lee, M. Li, B. Maher, D. Mudigere, M. Naumov,

M. Schatz, M. Smelyanskiy, X. Wang, B. Reagen, C. Wu, M. Hempstead, and X. Zhang. Recnmp: Accelerating personalized recommendation with near-memory processing. In *2020 ACM/IEEE 47th Annual International Symposium on Computer Architecture (ISCA)*, pages 790–803, 2020. doi: 10.1109/ISCA45697.2020.00070.

[62] M. Shoeybi, M. Patwary, R. Puri, P. LeGresley, J. Casper, and Bryan Catanzaro. Megatron-lm: Training multi-billion parameter language models using model parallelism. *ArXiv*, abs/1909.08053, 2019.

[63] Trishul Chilimbi, Yutaka Suzue, Johnson Apacible, and Karthik Kalyanaraman. Project adam: Building an efficient and scalable deep learning training system. In *11th USENIX Symposium on Operating Systems Design and Implementation (OSDI 14)*, pages 571–582, Broomfield, CO, October 2014. USENIX Association. ISBN 978-1-931971-16-4. URL <https://www.usenix.org/conference/osdi14/technical-sessions/presentation/chilimbi>.

[64] Zhihao Jia, Matei Zaharia, and Alex Aiken. Beyond data and model parallelism for deep neural networks. *SysML 2019*, 2019.

[65] Jakub M Tarnawski, Amar Phanishayee, Nikhil Devanur, Divya Mahajan, and Fanny Nina Paravecino. Efficient algorithms for device placement of dnn graph operators. *Advances in Neural Information Processing Systems*, 33, 2020.

[66] Assaf Eisenman, Maxim Naumov, Darryl Gardner, Misha Smelyanskiy, Sergey Pupyrev, Kim Hazelwood, Asaf Cidon, and Sachin Katti. Bandana: Using non-volatile memory for storing deep learning models. *Proceedings of Machine Learning and Systems*, 1:40–52, 2019.

[67] Jeremy Fowers, Kalin Ovtcharov, Karin Strauss, Eric Chung, and Greg Stitt. A high memory bandwidth fpga accelerator for sparse matrix-vector multiplication. In *International Symposium on Field-Programmable Custom Computing Machines*. IEEE, May 2014. URL <http://research.microsoft.com/apps/pubs/default.aspx?id=217166>.